Electrochemical and DFT studies of the oxidative decomposition of the trihydride complexes Cp*M(dppe)H3 (M = Mo, W) in acetonitrile

Rinaldo Poli, Miguel Baya, Rita Meunier-Prest, Suzanne Raveau

Electrochemical and DFT studies of the oxidative decomposition of the trihydride complexes Cp*M(dppe)H_3 (M = Mo, W) in acetonitrile

Rinaldo Poli,*[a] Miguel Baya,[a] Rita Meunier-Prest[b] and Suzanne Raveau[b]

Receipt/Acceptance Data **[DO NOT ALTER/DELETE THIS TEXT]**
Publication data **[DO NOT ALTER/DELETE THIS TEXT]**
DOI: 10.1039/b000000x [DO NOT ALTER/DELETE THIS TEXT]

A detailed electrochemical study of the oxidative decomposition of the trihydride complexes Cp*M(dppe)H_3 (M = Mo, W) in acetonitrile is presented. For the Mo complex, the decomposition occurs by four different pathways involving classical and non classical tautomers, whereas only the classical form is accessible for the W derivative. Each of the decomposition pathways has been quantitatively assessed by analyses of the linear sweep voltammograms. In addition to the previously established (*J. Am. Chem. Soc.*, **1999**, *121*, 2209-2225) deprotonation, disproportionation, and H_2 reductive elimination occurring via the nonclassical tautomer of the 17-electron complex $[Cp^*Mo(dppe)H_3]^+$ (obtained by oxidation at $E_{1/2}$ = -0.33 V vs. Ag/AgCl), a new decomposition pathway from the more stable classical tautomer have been identified following a second oxidation process. In addition, the oxidatively induced H_2 reductive elimination, previously evidenced only in THF or CH_2Cl_2, has been quantitatively assessed in MeCN. This process occurs preferentially by an associative mechanism (k = 0.020(4) $M^{-1}s^{-1}$) via the 19-electron $[Cp^*Mo(dppe)H(H_2)(MeCN)]^+$ intermediate and is therefore in direct competition with the disproportionation mechanism. The resulting 17-electron $[Cp^*Mo(dppe)H(MeCN)]^+$ product is further oxidized at ca. 0.2 V. The oxidation of $[Cp^*Mo(dppe)H_3]^+$ occurs at ca. 1.0 V and the resulting 16-electron $[Cp^*Mo(dppe)H_3]^{2+}$ complex immediately delivers a proton to starting material, giving $[Cp^*Mo(dppe)H_4]^+$ and $[Cp^*Mo(dppe)H_2]^+$. The latter coordinates MeCN in a rate determining step to afford $[Cp^*Mo(dppe)H_2(MeCN)]^+$. The mechanistic details are consistent with studies at different scan rates and different MeCN concentrations, and are backed up by DFT calculations.

Introduction

Transition metal hydride complexes have led to considerable attention both for practical and fundamental reasons such as hydrogen storage,[1] industrial catalysis,[2] the study of coordinated H_2 ligands (so called non-classical hydride complexes),[3-7] the existence of stable paramagnetic transition metal mono- and polyhydride complexes,[8] and so forth. We are interested in the kinetic stabilization of paramagnetic complexes and their further transformation to highly unsaturated reactive species. In this context, it is of fundamental importance to have a complete knowledge of the available decomposition mechanisms and to understand how they can be selectively affected by the ligand environment and other external parameters. In a previous paper,[9] we have shown that $[Cp^*Mo(dppe)H_3]^{+\bullet}$ decomposes according to three different pathways depending on conditions, all of them occurring via the nonclassical tautomer, $[Cp^*Mo(dppe)H(H)_2]^{+\bullet}$. These consist of (*i*) substitution of H_2 with a solvent molecule (only evidenced in THF or CH_2Cl_2); (*ii*) solvent assisted disproportionation, prevalent in MeCN; and (*iii*) deprotonation by excess Cp*M(dppe)H_3. The last two mechanisms have been elucidated by analyses of the cyclic and thin layer voltammograms of the first oxidation step of Cp*M(dppe)H_3 in MeCN. We present in this paper a more detailed investigation over a larger range of potentials covering the first and the second oxidation stages. This study reveals an additional electrochemical process that can be linked to the oxidatively induced H_2 substitution by MeCN, allowing its quantitative assessment. In addition, an additional pathway involves the more stable classical form of the 17-electron trihydride complex, following its further oxidation.

[a] *Laboratoire de Chimie de Coordination, UPR CNRS 8241, lié par convention à l'Université Paul Sabatier et à l'Institut National Polytechnique de Toulouse, 205 Route de Narbonne, 31077 Toulouse, France. Fax: +33-(0)561553003; Tel: +33-(0)561333195; E-mail: poli@lcc-toulouse.fr*
[b] *Laboratoire de Synthèse et d'Electrosynthèse Organométalliques, UMR CNRS 5188, Université de Bourgogne, Faculté des Sciences Mirande, 9 avenue Alain Savary, 21078 Dijon, France*
† Electronic Supplementary Information (ESI) available: Cartesian coordinates of all DFT optimized geometries (7 pages). See http://dx.doi.org/10.1039/b000000x/

Results and Discussion

This article mostly focuses on the complex electrochemical behavior of the molybdenum compound Cp*Mo(dppe)H_3. The related tungsten complex Cp*W(dppe)H_3 behaves in a much simpler fashion. Its study has helped in many occasions to clarify obscure issues related to the behavior of the molybdenum system. To simplify the notation, the Cp*M(dppe) moiety (M = Mo, W), is abbreviated as [M] except in the section titles, *e.g.* complex Cp*Mo(dppe)H_3 will be abbreviated as [Mo]H_3.

Voltammetric study of Cp*M(dppe)H_3 (M = Mo, W)

General features

The voltammogram of [Mo]H_3 in MeCN presents five redox systems over the potential range from –1 V to +1.5 V *vs.* Ag/AgCl, see Figure 1. These consist of a system A/A' which corresponds to the first oxidation of [Mo]H_3 ($E°_A$= -0.34 V), an irreversible peak B, a reversible system C/C' ($E°_C$ = 0.336 V), an irreversible peak D and a reversible system F/F' ($E°_F$ = 1.2 V).

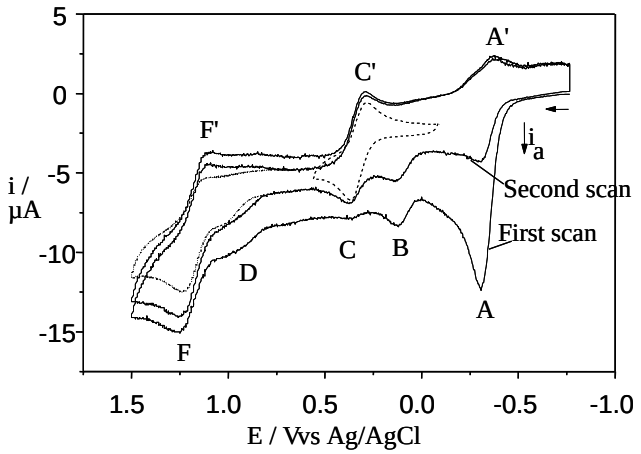

Figure 1 Two-cycle cyclic voltammogram of $[Mo]H_3$, $3.7x10^{-4}$ M in MeCN containing 0.2 M Bu_4NPF_6 at a scan rate of 0.2 Vs^{-1}. Superposition of the voltammograms of (— —) $[Cp^*MoH_2(dppe)(MeCN)]^+$ and (—•—) $[Cp^*MoH(dppe)(MeCN)_2]^{2+}$ under the same conditions.

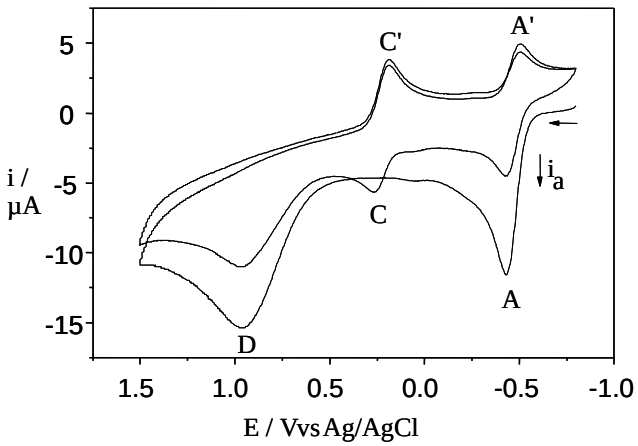

Figure 2 Two-cycle cyclic voltammogram of $[W]H_3$, $2x10^{-4}$ M in MeCN containing 0.2 M Bu_4NPF_6 at a scan rate of 0.6 Vs^{-1}.

The A/A' system has been previously investigated in detail in MeCN solution at various scan rates and concentrations, both by cyclic voltammetry and by thin-layer cyclic voltammetry.[9] A solvent-assisted disproportionation and a deprotonation of the one-electron oxidation product $[Mo]H_3^{+\bullet}$ by residual unoxidized $[Mo]H_3$ take place competitively. The disproportionation rate constant was obtained by analyzing the cyclic voltammetry results (k_{disp} = 3.98(9)x10^3 $M^{-1}s^{-1}$) while the deprotonation rate constant was derived from the thin-layer experiments (k_{dep} = 2.8(2)x10^2 $M^{-1}s^{-1}$). In the previous paper,[9] we have also shown that the stoichiometric chemical oxidation of $[Mo]H_3$ in MeCN leads to a mixture of $[Mo]H_2(MeCN)^+$ and $[Mo]H(MeCN)_2^{2+}$.

An independent electrochemical investigation of these two products in MeCN helps clarify some of the features of the complex voltammetric behavior of MoH_3. Both complexes exhibit reversible oxidation processes and, as expected, $[Mo]H_2(MeCN)^+$ is easier to oxidize (E° = 0.336V) than $[Mo]H(MeCN)_2^{2+}$ (E° = 1.2V). By superposition of the voltammograms recorded under the same experimental conditions, the C/C' couple in Figure 1 can be assigned to the reversible oxidation of $[Mo]H_2(MeCN)^+$, while F/F' corresponds to that of $[Mo]H(MeCN)_2^{2+}$. Species $[Mo]H_2(MeCN)^+$ is formed only after process D has taken place, because when the voltammetric measurement is carried out up to a switching potential of 0.5 V, the C/C' system is not observed on the reverse and second scans. On the other hand, peak B is present on the very first scan. Neither its relative intensity nor its irreversibility in subsequent multiple scans are affected by the occurrence of process D. In comparison with complex $[Mo]H_3$, the behavior of $[W]H_3$ in MeCN is much simpler, see Figure 2. Peak B is quasi non-existent and system F/F' is not observed whatever the sweep rate in the potential range studied (from –1 V to +1.5 V *vs.* Ag/AgCl). Like for the analogous molybdenum system, the C/C' process ($E°_C$ = 0.225 V) is not observed when the scan is reversed before the occurrence of process D.

Our previous investigations[9] have shown that the greater electron richness of W relative to Mo disfavors the chemical decomposition of $WH_3^{+\bullet}$ which could in fact be isolated from a CH_3CN/Et_2O solution. Its X-ray structure shows a classical trihydride geometry (as opposed to a *nonclassical* monohydride(dihydrogen) structure, $[W](H)(H_2)^{+\bullet}$). The stability of $[W]H_3^{+\bullet}$ in MeCN suggests that peak D corresponds to the oxidation of $[W]H_3^{+\bullet}$ to $[W]H_3^{2+}$. This is confirmed by an independent cyclic voltammetric study of complex $[W]H_3^{+\bullet}$, *vide infra*. Thus, the similarity of peak D for the Mo and W systems (*cf.* Figure 1 and Figure 2) indicates that the oxidized Mo system, $[Mo]H_3^{+\bullet}$, also adopts a *classical* trihydride structure and is oxidized irreversibly to species $[Mo]H_3^{2+}$ at peak D. An internal electronic rearrangement from the classical Mo^V trihydride to a nonclassical Mo^{III} hydride-dihydrogen complex would be expected to lead to more dramatic differences in the cyclic voltammogram, as shown in previous studies.[10] DFT calculations (*vide infra*) agree with a classical form for the Mo complex, at least at the oxidation state level $[Mo]H_3^+$.

When the scan rate is increased, the voltammogram of $[Mo]H_3$ evolves (e.g see Figure 3 at v = 8 V s^{-1}) to become similar to that of $[W]H_3$, *i.e.* peaks B and F/F' disappear while the current of the cathodic peak A' increases. At the same time, peak D shifts towards more positive values. To summarize the observations made so far, we can identify two independent phenomena. The first one, prevalent at high scan rates, is the development of process C/C' (reversible oxidation of $[Mo]H_2(MeCN)^+$) after the formation of $[Mo]H_3^{2+}$ at D. The second one, most visible at slow scan rates, consists of the development of processes B and F/F', which may or may not be related to each other. We shall examine the first phenomenon in the next section and will return to processes B and F/F' in the following one.

Analysis of the A/A', C/C', and D processes.

As seen above, the C/C' system is observed only after the second oxidation process leading to $[Mo]H_3^{2+}$. In addition, an analysis of Figure 2 and Figure 3 shows that, upon running two consecutive cycles, the height of peak A in the second scan is reduced to one half that of the first scan for the W compound while a smaller but nevertheless significant decrease is observed for the Mo compound (A/C = 1 for W; 3 for Mo; this ratio becomes 1 also for the Mo compound at slower scan rates, see Figure 1). From these observations, we

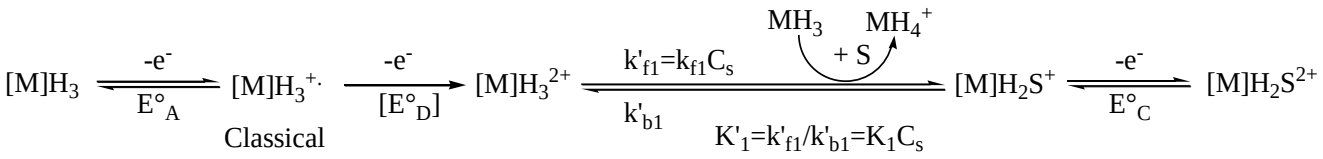

Scheme 1

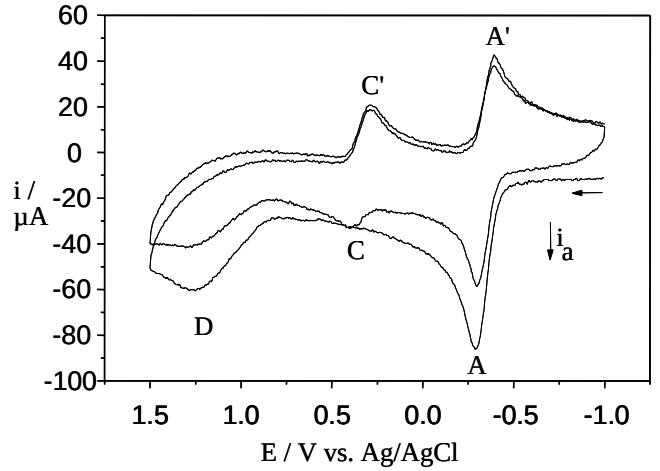

Figure 3 Two-cycle cyclic voltammogram of $[Mo]H_3$, $4x10^{-4}$ M in MeCN containing 0.2 M Bu_4NPF_6 at a scan rate of 8 Vs^{-1}.

conclude that the $[M]H_3^{2+}$ complex formed in the second oxidation stage is involved in a chemical reaction leading to $[M]H_2(MeCN)^+$ (this is in accordance with the irreversibility of system D and with its potential shift as the scan rate increases) and that two $[M]H_3$ molecules have been involved in the global mechanism, see Scheme 1. The overall scheme corresponds therefore to an EECE process. The chemical step must obviously be slower for the Mo than for the W system, since the height of peaks A and A' in the second scan is reduced to one half that in the first scan only at slow scan rates (*cf.* Figure 1 and Figure 3).

The proposed deprotonation of the doubly oxidized complex by the starting compound has ample precedents in the literature[8] and is in accordance with the known acidity increase[11] on going from the 18 to the 17 and further to 16-electron hydride complexes. According to our previous chemical study,[9] complex $[M]H_4^+$ evolves to generate additional $[M]H_2(MeCN)^+$ by the replacement of two hydride ligands (reductively eliminating to afford H_2) by a solvent molecule. This reaction, however, is slow on the time scale of the cyclic voltammetric experiment and consequently does not contribute to the shape of the cyclic voltammetric response. Furthermore, $[M]H_4^+$ is not electroactive in the potential range –1 to +1.5 V (vs. Ag/AgCl) and therefore no kinetic data on this chemical step would be accessible from the electrochemical experiments.

In order to confirm the involvement of MeCN in the EECE mechanism of Scheme 1, we have studied the electrochemical response of $[Mo]H_3$ in various THF/MeCN mixtures. In pure THF, the oxidation of $[Mo]H_3$ induces a slow dihydrogen reductive elimination ($k = 0.0016$ min^{-1})[9] that cannot be seen on the cyclic voltammetry time scale. In addition, the decomposition modes by disproportionation and proton

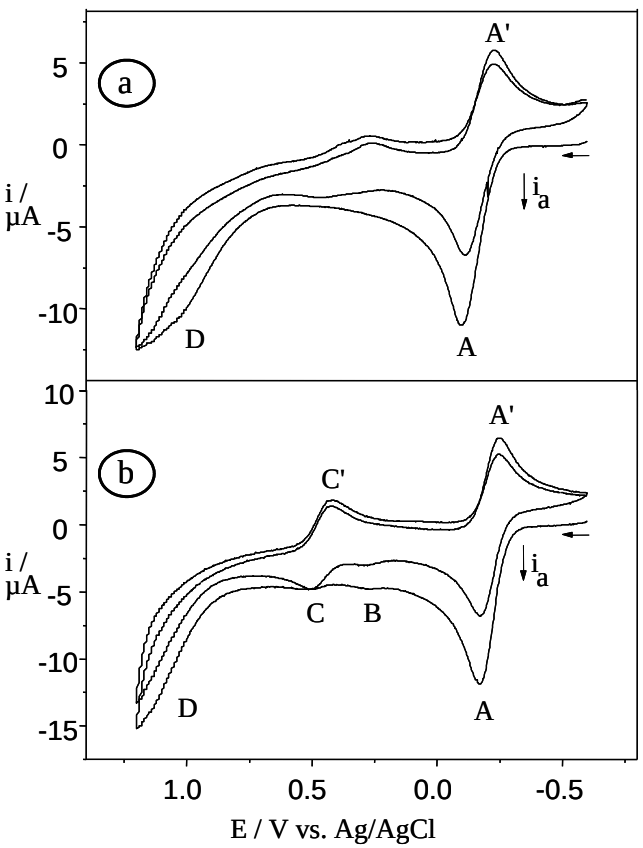

Figure 4 Two-cycle cyclic voltammogram of $[Mo]H_3$, $1.5x10^{-4}$ M in THF/MeCN mixtures containing 0.2 M Bu_4NPF_6 at a scan rate of 1 Vs^{-1}; (a): C_{MeCN} = 0 M, (b): 3.2 M.

transfer[9] are also not observable in this solvent at the scan rates used for this study. Consequently, the voltammogram presents only the reversible system A/A' corresponding to the first oxidation followed by the second oxidation (peak D), see Figure 4, part a. As a matter of fact, a low intensity feature also appears at a potential close to that characteristic of the reversible $[Mo]H_2(MeCN)^+$ oxidation, but peaks C/C' appear as a well defined reversible wave only after MeCN is gradually added to the solution. We tentatively attribute this additional peak to a trapping process by the THF solvent according to Scheme 1, but the resulting $[M]H_2(THF)^+$ product is presumably less stable. Peak B is completely absent in pure THF.

The A/A' peak potential values do not depend on the MeCN concentration up to *ca*. 1.7 M, demonstrating that no thermodynamically favorable interaction with the solvent occurs after the first oxidation process. At higher MeCN concentrations, the whole A/A' system starts to shift toward less positive potentials with a slope of –200 mV / log C_{MeCN}. This shift is probably caused by solvation effects, as has

previously been shown for other similar cation-solvent interactions.[12] The slight A/A' current increase on going from THF to MeCN may be attributed to the low dielectric constant of THF (ε_{THF} = 7.4) compared to that of MeCN (ε_{MeCN} = 37).[13] This makes the THF solutions quite resistive inducing a bigger gap between the anodic and cathodic peaks.

The C/C' couple appears immediately at the lowest C_{MeCN} used (*i.e.* 0.038 M). Upon further increasing C_{MeCN}, the current and the peak potentials of these peaks do not further change. This is due to the large excess of MeCN compared to $[Mo]H_3^{2+}$ and to the fast chemical transformation leading to $[Mo]H_2(MeCN)^+$. Finally, the solvent addition to $[Mo]H_3^{2+}$ must has an influence on the evolution of peak D with the MeCN concentration.[14] For a mechanism of the type shown in Equations 1 and 2, (S = redox inactive reagent; ν_X and ν_S = stoichiometric coefficients), the theory shows that the peak potential should vary linearly with the logarithm of the S concentration according to Equation 3,[15] where ρ_X and ρ_S are the reaction orders.

$$X - ne^- \rightarrow X^{n+} \quad (1)$$

$$\nu_X X^{n+} + \nu_S S \rightarrow \text{Products} \quad (2)$$

$$\frac{\partial E_p}{\partial \log C_S} = \frac{\rho_S}{(\rho_X + 1)} \frac{60}{n} \frac{T}{302} \quad (3)$$

A plot of the peak potential Ep_D as a function of log C_{MeCN} is shown in Figure 5. For each scan rate, peak D shifts towards more positive values as C_{MeCN} increases with a slope of approximately 30 mV per log unit (Figure 5 and Table 1). This is consistent with $\rho_X = \rho_S = 1$ (Equation 3, n = 1), *i.e.* the chemical reaction is first order in both $[Mo]H_3^{2+}$ and MeCN, in agreement with the formation of $[Mo]H_2(MeCN)^+$ as postulated in Scheme 1. This observation excludes that the chemical process consists of an irreversible and rate determining proton transfer followed by a fast solvent coordination (Scheme 2, path *a*). However, either a rate determining solvent coordination followed by proton transfer (path *b*) or a fast (reversible or irreversible) proton transfer followed by an irreversible and rate determining solvent coordination (path *c*) would be compatible with the results.

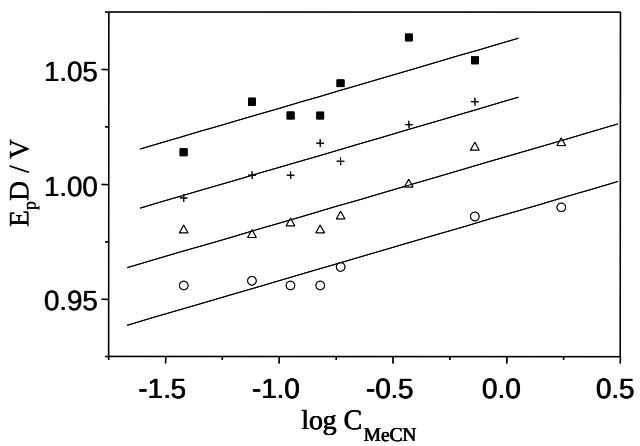

Figure 5 Variations of E_{pD} as a function of log C_{MeCN} extracted from the experimental voltammograms of $[Mo]H_3$, 1.5×10^{-4} M in THF/MeCN mixtures containing 0.2 M Bu_4NPF_6 at different scan rates: (■) 0.2 Vs^{-1}, (×) 0.1 Vs^{-1}, (△) 0.06 Vs^{-1}, (○) 0.04 Vs^{-1}.

Table 1 Slopes of the variations of the peak potential of process D for compound $[Mo]H_3$ as a function of log C_{MeCN} (Figure 5)

v / Vs^{-1}	$(\partial E_{pD} / \partial \log C_{MeCN})$ / mV	Regression coefficient
0.2	34 (8)	0.88
0.1	32 (4)	0.97
0.06	29 (4)	0.93
0.04	25 (4)	0.94

An additional dichotomy in relation to the proton transfer process must be considered. When complex $[Mo]H_3^{2+}$ (or its MeCN adduct) furnishes its proton to $[Mo]H_3$, it may adopt either a classical or a nonclassical form. It has been shown in a number of cases that the kinetic acidity is greater for a dihydrogen complex even when the thermodynamic acidity is greater for the dihydride tautomer.[16-18] Thus, we must consider the possibility that the $[Mo]H_3^{2+}$ species delivers the proton only after an internal rearrangement to the nonclassical form, even if this may be thermally less favored. Any such rearrangement would consist of a (reversible) first order process and would not affect the overall electrochemical and kinetic behavior. The relative energy of the two $[Mo]H_3^{2+}$ isomers will be analyzed later in the DFT section.

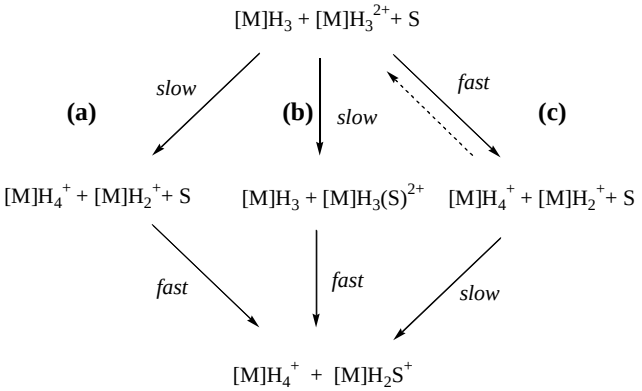

Scheme 2

Cyclic voltammetry of $[Cp^*W(dppe)H_3]^+$

Further confirmation of the mechanism shown in Scheme 1 comes from the cyclic voltammogram of complex $[W]H_3^+$. The molybdenum analogue, as stated above, is not a stable compound and therefore cannot be studied under analogous conditions. The compound shows the expected reversible A'/A process in the reductive direction and the irreversible peak D in the oxidative direction. When the scan is extended on the positive potentials side to +0.8 V to encompass process C/C', see Figure 6(a), no significant redox activity is observed at the C/C' potential, confirming that complex $[W]H_2(MeCN)^+$ does not form rapidly upon spontaneous decomposition of $[W]H_3^+$. Further extension of the scan to +1.5 V gives rise to the appearance of the C/C' peaks at low intensity after transit over the irreversible D peak, and a slight decrease of the A/A' peak intensities, see Figure 6(b). However, peaks C and C' do not reach the same intensity as

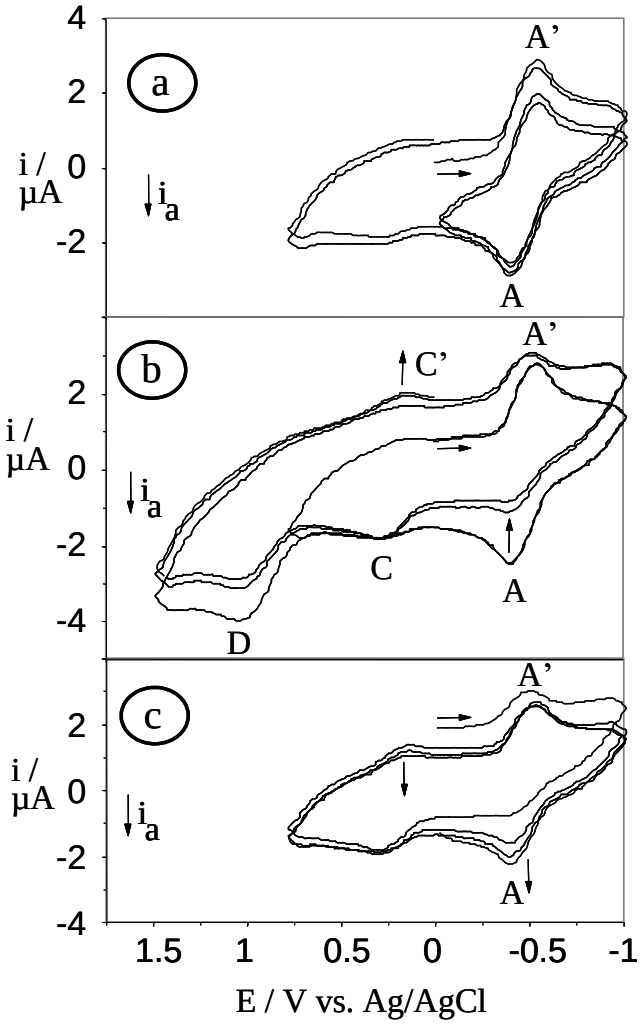

Figure 6 Multiple-cycle cyclic voltammogram of $[W]H_3^+$, $1.4x10^{-3}$ M in MeCN containing 0.2 M Bu_4NPF_6 at a scan rate of 50 Vs^{-1}; (a): scans 1-3 between 0 and -1 V, then scans 4-5 between -1 and +0.8 V, (b): scans 5-6 between -1 and +0.8, then scans 7-9 between -1 and +1.5 V; (c): scans 9-12 between -1 and +0.8 V.

peak A', a very different result from that of the experiment carried out on $[W]H_3$ (Figure 2). The obvious reason for this outcome is that complex $[W]H_3$ is not present in the bulk of the solution; it is only generated in the diffusion layer at lower concentrations from $[W]H_3^+$ during the reductive scan (peak A'). Therefore, the reaction between $[W]H_3^{2+}$ (produced at D) and $[W]H_3$ (produced at A'), leading to $[W]H_2(MeCN)^+$ according to Scheme 1, occurs to a lower extent. A continuation of the same experiment, but switching again the potential scan at +0.8 V, allows a recovery of the reversible A/A' process intensity, while the C/C' peaks slowly fade away as shown in Figure 6(c). Given the close correspondence of the peak potentials for all processes of the Mo and W complexes, the behavior established for the W complex may safely be extrapolated to the Mo analogue. Therefore, the combination of the experiments in mixed THF/MeCN solvent for $[Mo]H_3$ (Figure 4) and the voltammograms of $[W]H_3$ (Figure 2) and $[W]H_3^+$ (Figure 6) in pure MeCN establish unambiguously that complex $[M]H_2(MeCN)^+$, responsible for process C/C', is only generated upon the simultaneous presence of $[M]H_3$, $[M]H_3^{2+}$, and MeCN.

Analysis of process B

As shown previously, process B becomes predominant only at low scan rates and its presence is independent from the EECE process examined in the previous section. In order to understand the origin of this process, more detailed voltammetric investigations were carried out up to a switching potential of 0.5 V vs Ag/AgCl. The investigations carried out in mixed THF-MeCN solvent show that the intensity of this peak increases proportionally with C_{MeCN}. Therefore, the compound oxidized in B must result from the reaction of MeCN with $[Mo]H_3^{+\bullet}$, *i.e.* we have a chemical-electrochemical (CE) mechanism, the chemical reaction preceding the electrochemical one being a solvent addition process. We can consider three possibilities for the nature of this chemical process. The first one (pathway *a* in Scheme 3) is the direct addition of MeCN to the classical 17-electron $[Mo]H_3^{+\bullet}$ complex leading to a 19-electron $[Mo](MeCN)H_3^{+\bullet}$ product which would then be oxidized at E_B. There are literature reports underlining solvent addition equilibria to 17-electron complexes, to afford "19-electron" species.[19-23]. As we shall see below, the computational studies do not support this mechanism. The second one (pathway *b* in Scheme 3) is the addition of MeCN to the 17-electron complex after rearrangement to the nonclassical isomer, $[Mo]H(H_2)^{+\bullet}$, leading to the 19-electron $[Mo](MeCN)H(H_2)^{+\bullet}$ product. Note that this is the same proposed intermediate for the

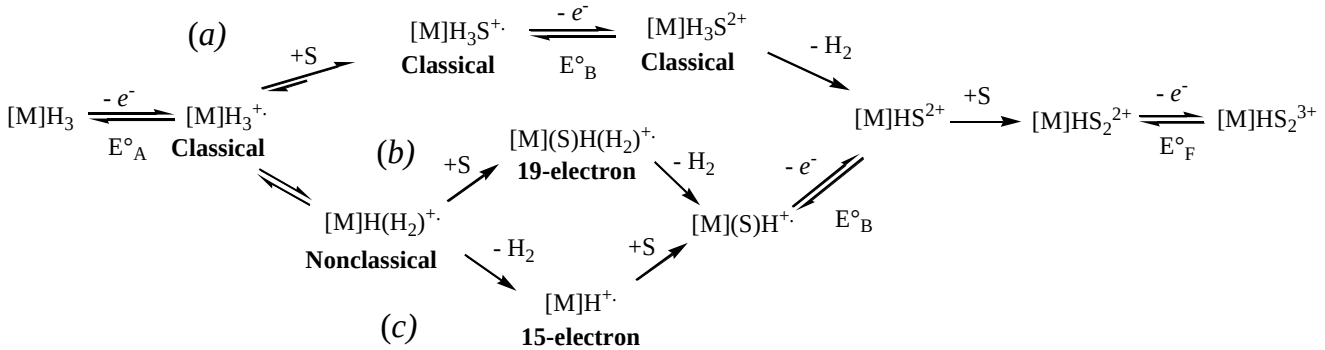

Scheme 3

disproportionation mechanism, which requires that this compound is oxidized at a lower potential than E_A. Therefore, this intermediate cannot be responsible for peak B. However, H_2 loss may take place competitively with the disproportionation process, leading to the 17-electron $[Mo](MeCN)H^{+\bullet}$ complex, which may be the species responsible for peak B. The overall process from $[Mo]H(H_2)^{+\bullet}$ to $[Mo](MeCN)H^{+\bullet}$ is an associative ligand substitution. The third possibility (pathway *c* in Scheme 3) is the same ligand substitution process as in pathway *b*, but proceeding via a dissociative mechanism involving the 15-electron $[Mo]H^+$ intermediate. The combination of the experimental and computational evidence, *vide infra*, agrees best with pathway b.

A slow-scan voltammetric investigation of the W compound reveals a small peak at 0.104 V (see Figure 7). This peak is in the same region as peak B for the Mo system (*cf.* with Figure 1), but is visible only at very small intensity and only at very slow scan rates. For the Mo complex, on the other hand, the intensity of the B peak may become as large as that of the A peak (*vide infra*). Thus, if path (*a*) of Scheme 3 takes place, we must assume that the reason for its low intensity for the W system is a slower MeCN addition rate or a less favorable solvent addition equilibrium leading to classical $[W]H_3(MeCN)^{+\bullet}$. These propositions do not have an easy rationalization (see also the DFT results below). If the decomposition follows instead path (*b*) or (*c*) of Scheme 3, on the other hand, it is relatively easy to explain the lower intensity for the W system on the basis of the different position of the classical-nonclassical equilibrium (more heavily shifted toward the classical isomer for the tungsten system). Note that peak B is not clearly visible at significant intensity for the voltammogram of complex $[W]H_3^+$ (Figure 6), proving that its low intensity has a thermodynamic origin. For the Mo complex, on the other hand, peak B increases as the scan rate decreases (compare Figure 1 and Figure 3), indicating a kinetic control.

The relative intensity of peak B compared to that of A for the Mo system has been quantitatively studied as a function of the scan rate and of the acetonitrile concentration. The intensity of peaks A (i_{aA}) and B (i_{aB}) are proportional to the amounts of $[Mo]H_3$ and of the $[Mo]H_3(MeCN)^{+\bullet}$ (pathway *a*) or $[Mo]H(MeCN)^{+\bullet}$ (pathways *b* and *c*) complex being generated in the chemical step. Thus, the fraction ρ of $[Mo]H_3^{+\bullet}$ which is converted to the solvent adduct is given by i_{aB}/i_{aA}. Figure 8 presents the variation of ρ as a function of $\log(v/C_{MeCN})$. The curve has a sigmoidal form varying from 1 for small scan rates and/or large MeCN concentrations to 0 for fast scan rates and/or little MeCN concentrations. The inverse dependence on v and C_{MeCN} clearly shows that the chemical step has a first order dependence on the acetonitrile concentration. This can be easily rationalized on the basis of pathways *a* and *b*, where the slow step is likely to be the MeCN addition to the 17-electron classical or noclassical trihydride complex, respectively. On the other hand, the H_2 elimination in pathway *c* precedes the MeCN coordination and thus probably represents the reaction slow step. Therefore, a first order dependence on MeCN is not anticipated for pathway *c*.

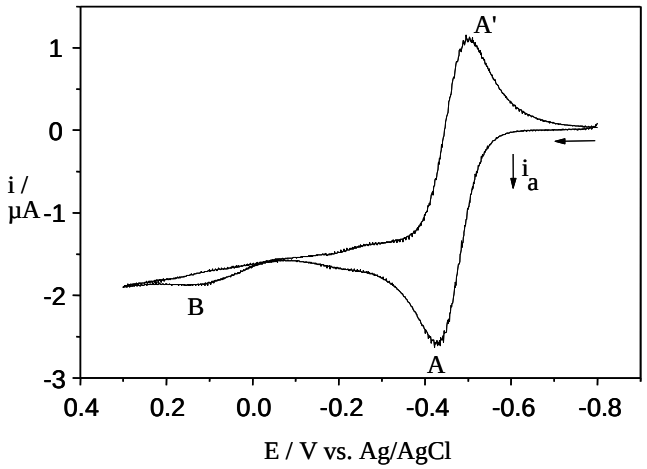

Figure 7 Cyclic voltammetry of $[W]H_3$, $2x10^{-4}$ M in MeCN + 0.2 M Bu_4NPF_6, v = 0.016 Vs^{-1}.

As mentioned in section 3.1, process A/A' is fully reversible and no peak B is observed when MeCN is not present (ρ = 0). For a given scan rate, the time available for the chemical reaction to occur corresponds to the time required to go from E_{pA} to E_{pB}, as shown in Equation 4. At any time, the $[Mo]H_3(MeCN)^{+\bullet}$ or $[Mo]H(MeCN)^{+\bullet}$ concentration is described by Equation 5 where k_{obs} is the pseudo-first order forward rate constant of the chemical process (see Scheme 3). The scan rate for which ρ = 0.5, *i.e.* when half the amount of the electrogenerated $[Mo]H_3^{+\bullet}$ reacts with MeCN, provides the reaction half-life from Equation 6 and the chemical rate constant from Equation 7. According to Figure 8, there are three points in the interval $0.45 < \rho < 0.55$. They are collected in Table 2. The mean rate constant thus obtained is $k = 0.020(4)$ M^{-1} s^{-1}.

$$t = \frac{|E_{pA} - E_{pB}|}{v} = \frac{\Delta E_p}{v} \qquad (4)$$

$$\rho = \frac{i_{aB}}{i_{aA}} = \exp(-k'_{f2}t) \qquad (5)$$

$$\rho = 0.5 = \exp(-k'_{f2}t_{1/2}) \qquad (6)$$

$$k'_{f2} = \frac{Ln2}{t_{1/2}} \qquad (7)$$

The electrochemical process B is irreversible (no cathodic peak is observed in the reverse scan). The shift of the peak potential as a function of the scan rate and $[Mo]H_3$ concentration confirms that this process is followed by a rapid chemical reaction. The potential E_{pB} is not affected by the concentration but varies linearly with log v with a slope of approximately 30 mV / log v unit (Figure 9). This is characteristic of a charge transfer followed by a first order chemical reaction.[24] The follow-up processes for this decomposition pathway could either be a H_2 reductive elimination and replacement by a solvent molecule (in case of pathway *a*), or a simple solvent addition (pathway *b*). In each

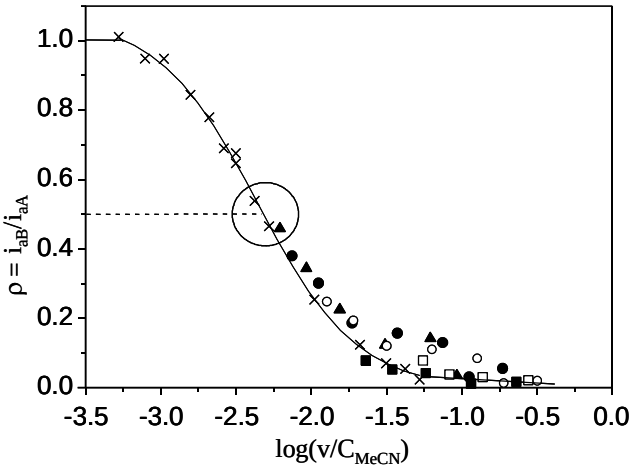

Figure 8 Intensity ratio of peaks B and A (i_{aB}/i_{aA}) for $[Mo]H_3$ as a function of $\log(v/C_{MeCN})$. C_{MeCN} = (×) 19 M, (▲) 6.5 M, (□) 5.4 M, (○) 3.2 M, (■) 1.7 M, (□) 1.4 M. The 3 values near i_{aB}/i_{aA} = 0.5 are reported in Table 2.

case, the process leads to the formation of complex $[M]H(MeCN)_2^{2+}$ which is responsible for the electrochemical processes F/F'.

The complete scheme

By analysis of the voltammogram over a large range of potentials, we have found a new oxidative decomposition pathway for $[Mo]H_3$ and $[W]H_3$ in MeCN. Furthermore, the oxidatively induced H_2 reductive elimination, which was previously evidenced only in THF and CH_2Cl_2, has been linked to the previously undetected peak B. The detailed analysis of this electrochemical process has allowed us to quantify this decomposition pathway in MeCN. As already mentioned, the DFT calculations provide evidence in favor of pathway *b* or *c* of Scheme 3 and against pathway *a*, whereas the experimentally determined first order dependence on C_{MeCN} for the rate of formation of the electroactive species $[Mo]H(MeCN)^{+\bullet}$ favors pathways *a* and *b* over pathway *c*. The common denominator of the two results is pathway *b*. Therefore, the complete scheme shown in Scheme 4 is based on this mechanistic hypothesis.

Pathway I is the newly discovered decomposition path, which takes place after further oxidation of the 17-electron classical trihydride $[Mo]H_3^{+\bullet}$. The previously established pathways (deprotonation, disproportionation, and H_2 elimination) are indicated as II-IV. To briefly summarize the essential mechanistic interpretation of our previously reported results, all three decomposition pathways II-IV are accessed via the rearrangement of $[Mo]H_3^{+\bullet}$ to its nonclassical tautomer, $[Mo]H(H_2)^{+\bullet}$, which then evolves in different ways depending on conditions. The newly determined rate of the dihydrogen dissociation process (pathway IV; average k_{obs} = 0.34 s^{-1} in the pure solvent; k = 0.020(4) $M^{-1}s^{-1}$) is much faster than the pseudo-first order rates in THF (k_{obs} = $2.7(2)\cdot10^{-4}$ s^{-1} at 0°C) and CH_2Cl_2 (k_{obs} = $2.1(1)\cdot10^{-3}$ s^{-1} at 0°C).[9] The dependence of the rate on the solvent nature is in line with the higher nucleophilicity of MeCN relative to CH_2Cl_2 and THF and with the associative nature of this process. It is to be noted that the disproportionation and reductive elimination pathways III and IV share the common intermediate $[Mo](S)H(H_2)^{+\bullet}$. For S = MeCN, the disproportionation reaction (k_{disp} = $3.98(9)\text{x}10^3$ $M^{-1}s^{-1}$)[9] is ca. 5 orders of magnitude faster than the H_2 replacement by MeCN, explaining why the direct H_2 elimination was not previously evidence in this solvent. In the current experiment, it is highlighted only thanks to the low concentration of $[Mo]H_3^{+\bullet}$ relative to the MeCN solvent in the diffusion layer, especially for the experiments carried out at slower scan rates. The 18-electron $[Mo]H(H_2)S^{2+}$ species is a proposed intermediate of the disproportionation pathway and evolves to the other observed product $[Mo]HS_2^{2+}$, responsible for peak F, by replacement of H_2 with a solvent molecule. The deprotonation pathway (II) originates from the high kinetic acidity of the dihydrogen ligand in complex $[Mo]H(H_2)^{+\bullet}$. This is therefore deprotonated when a strong base (*e.g.* the unoxidized trihydride complex $[Mo]H_3$) is present, leading to the 17-electron species $[Mo]H_2$. The latter is presumably further oxidized by $[Mo]H_3^{+\bullet}$ (since its oxidation potential is likely to be lower than E_A) and trapped by a solvent molecule, yielding the observed product $[Mo]H_2S^+$ which is responsible for peak C. The necessary rearrangement to the nonclassical structure as a prerequisite for pathways II, III and IV nicely explains the stability of the tungsten analogue $[W]H_3^{+\bullet}$, since its more basic character relative to molybdenum makes the rearrangement to the dihydrogen complex energetically more difficult. The results of computational studies shown in the next few sections serve to back up the above assumptions and to verify the self-consistency of the mechanism proposed in Scheme 4.

Table 2 Experimental values of the rate constant of the reaction of $[Mo]H_3^{+\cdot}$ with MeCN (Scheme 3), obtained from Figure 8 when $0.45<\rho<0.55$.

Log (v/C_S)	v / Vs^{-1}	C_{MeCN} / M	ΔE_p / V	$t_{1/2}$ eqn. (10)	k_{obs} / s^{-1} eqn. (14)	k / $M^{-1}s^{-1}$ eqn. (12)
-2.376	0.08	19	0.444	5.55	0.305	0.016
-2.279	0.1	19	0.446	4.46	0.38	0.020
-2.21	0.04	6.5	0.436	10.9	0.155	0.024
					Mean value	**0.020(4)**

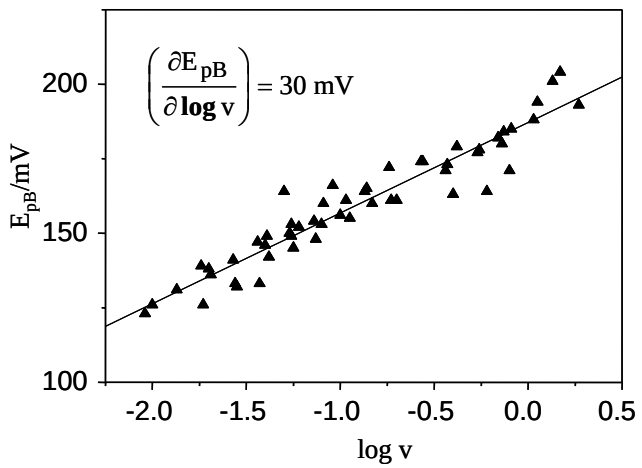

Figure 9 Variations of E_{pB} as a function of log v extracted from the experimental voltammograms of $[Mo]H_3$ in MeCN + 0.2 M Bu_4NPF_6.

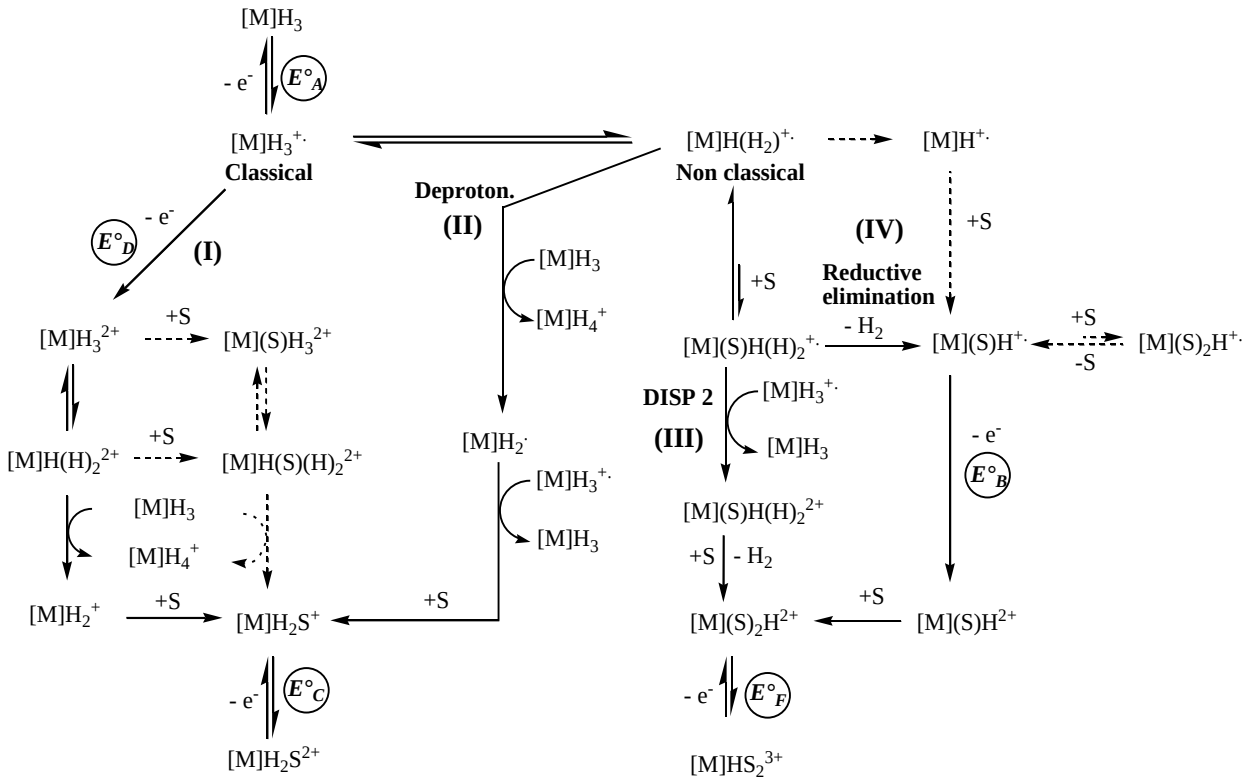

Scheme 4

Geometry optimization of key intermediates.

The geometry optimizations were carried out by DFT methods with the B3LYP functional and the standard LANL2DZ basis set, which was proven suitable for organometallic compounds of the type studied here, affording results within < 5 kcal/mol of the experiment.[25, 26] Most calculations were carried out on model systems where dpe (1,2-diphosphinoethane, $H_2PCH_2CH_2PH_2$) was used in place of dppe and Cp in place of Cp*. A larger calculation which included the real dppe ligand, but with the Cp* ligand still modeled by Cp, was carried out for the 17-electron trihydride system only. The relevant optimized parameters of the most stable structures are shown in the various Figures. The atomic coordinates for all optimized structures are available as Supporting Information. Some of the species described here [notably the neutral $CpMoH_3$(dpe) and $CpMoH(H_2)$(dpe) complexes, and the protonated complex $CpMoH_4(dpe)^+$] have also been calculated at a very similar level of theory as part of a different study, focused on hydrogen bonding and proton transfer.[27] They have been recalculated in the present study in order to compare their relative energy with those of the new calculations at the same theory level. The results do not differ significantly from those of the other study. Key calculations have also been carried out with the PCM,[28] to simulate the effect of the MeCN solvent. As will be shown, this affects the processes where a charge redistribution is involved.

The 17-electron $CpMoH_3(dpe)^{+\bullet}$ and $CpMoH_3(dppe)^{+\bullet}$ systems.

One key question for this investigation is the energy difference between the classical (*C*) and nonclassical (*NC*) tautomers of the 17-electron trihydride species obtained by oxidation of compound $[Mo]H_3$. The results for the simpler model systems are shown in Figure 10. Both *C* and *NC* structures are localized as distinct minima on the potential energy surface. In line with expectations (see above), the *C* form is found to be the more stable one, although by only 1.9 kcal/mol relative to the *NC* isomer. An analogous calculation on the two tautomers for the 18-electron neutral species shows an energy difference of 5.7 kcal/mol in favor of the *C* form. This is in line with the expected relative stabilization of the classical form as the metal center becomes electron-richer.[29, 30]

The optimized geometries for the 17-electron *C* and *NC* species are rather similar with each other and with those previously found experimentally (L_2 = dppe) and by DFT optimization (L_2 = dpe) on the classical tungsten analogue, $CpWH_3L_2^{+\bullet}$.[9] The most relevant geometric parameters are shown in Figure 10. As expected, the Mo-H distances for the two H atoms that participate to the rearrangement lengthen on going from the classical isomer to the transition state, while the H-H bond starts to form. The other Mo-H bond, on the other hand, becomes shorter during the rearrangement.

The transition state for this *C*/*NC* tautomerization process (*TS*) has also been optimized. This point lies higher than the classical minimum by only 3.2 kcal mol^{-1}. Therefore, it can be predicted that the interconversion between the two isomers will be very rapid and will not limit the rates of the H_2 elimination, deprotonation, and disproportionation processes. This is consistent with the previous experimental findings. In terms of free energy, the *NC* geometry is estimated 1.3 kcal mol^{-1} higher than the *C* geometry, whereas *TS* is 1.9 kcal mol^{-1} higher . If the calculated energetic parameters are assumed to be valid also for the real Cp*/dppe system, we can estimate

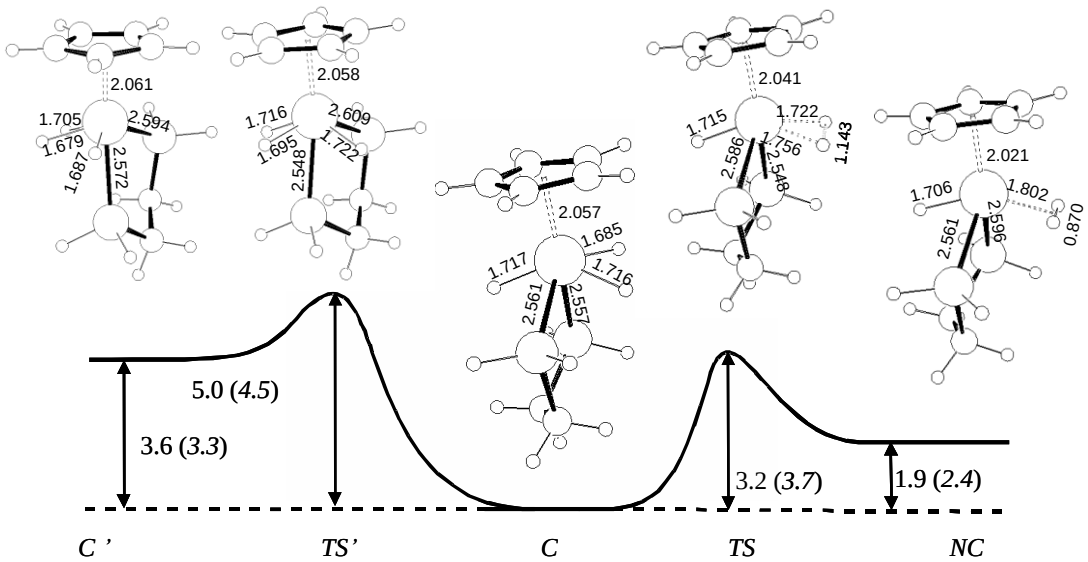

Figure 10 B3LYP/LANL2DZ-optimized geometries and gas-phase relative energies (MeCN solution values in parentheses) in kcal mol^{-1} for $[CpMoH_3(H_2PCH_2CH_2PH_2)]^{+\bullet}$.

that ca. 90 % of the 17-electron trihydride adopts the classical form at equilibrium, while the rate of transformation of $MoH_3^{+\bullet}$ to the nonclassical isomer $MoH(H_2)^{+\bullet}$ would be > 10^{11} s^{-1}. Therefore, this rearrangement does not limit the rate of the decomposition processes involving the nonclassical intermediate. Note also that the energy differences do not change significantly on going from the gas phase to the MeCN conditions (Figure 10).

A second classical local minimum (*C'*) was found at a higher energy (3.6 kcal/mol). Its geometry can be best described as a pseudo pentagonal bipyramid, the center of the Cp ring and one P donor occupying the axial positions and one equatorial position (between one P and one H ligand) being vacant. The transition state between the two classical tautomers (*TS'*) is located 5.0 kcal/mol above the absolute minimum. Its structure is approximately midway between those of *C* and *C'*, the three H ligands and the equatorial P atom being close to a square planar arrangement. It is easy to see how the interconversion of isomers *C* and *C'* allows the rapid exchange of the inequivalent hydride ligands, explaining the shape of the experimental EPR spectrum of complex $[Mo]H_3^+$, which shows coupling to three equivalent H nuclei.

The calculation on the larger dppe system did not change the picture dramatically. The classical *C* structure still results the most stable one, with the non classical form *C'* now being higher by 5.2 kcal mol^{-1} and the transition state *NC* by 5.3 kcal mol^{-1}.

The 16-electron $CpMoH_3(dpe)^{2+}$ system.

This dicationic species is a model for the double oxidation product of pathway I in Scheme 4. As mentioned above, an increase in metal oxidation state should favor the nonclassical tautomer by way of a less effective back-donation from the metal center to H_2. Indeed, this expectation is verified by the computational results. The relevant energetic and structural information is presented in **Figure 11**. The situation is further complicated here by the possibility for each of the forms (classical and nonclassical) to adopt either the singlet or the triplet spin state, as well as by additional stereoisomerism. Several species are found at comparable energy. The most stable classical structure [**Figure 11**(a)] is a singlet species whose geometry is very close to that of the higher energy classical tautomer of the 17-electron monocation (*C'*) in Figure 10. The stereoisomer having the open equatorial site between two H atoms is found 10.2 kcal/mol higher in energy. All attempts to find a local minimum for a classical structure in the triplet state led to the nonclassical isomers.

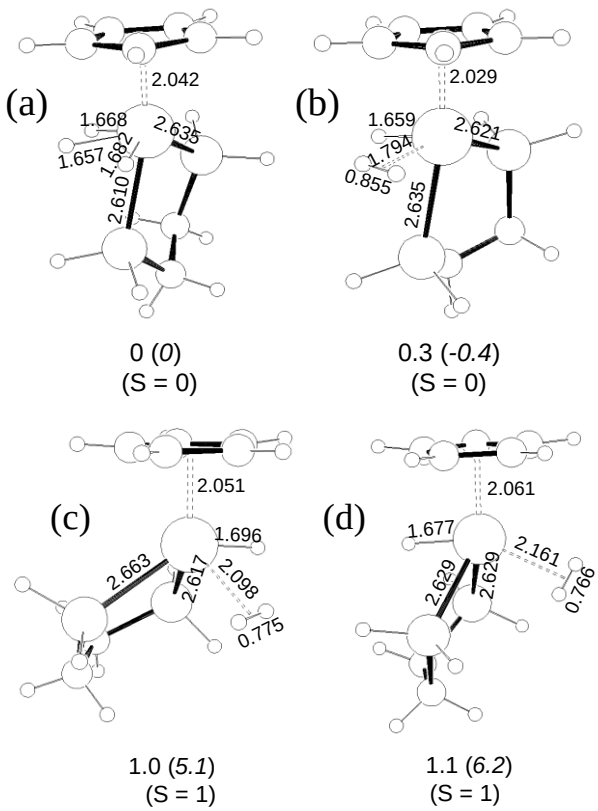

Figure 11 B3LYP/LANL2DZ-optimized geometries and relative gas phase (MeCN solution) energies in kcal mol^{-1} for $[CpMoH_3(H_2PCH_2CH_2PH_2)]^{2+}$.

Three different nonclassical species (one singlet and two triplets) are found to be close in energy to the above discussed classical species. They are all slightly less stable than the classical one in the gas phase. Of these, the singlet [**Figure 11**(b)] is slightly more stable in MeCN solution. This species has a geometry based on a distorted pseudo-octahedron with an unfilled equatorial position. Its formation from the most stable classical form can be easily viewed as the coming together of the two H ligands opposite to the equatorial P atom, while all other ligands remain essentially unchanged. This interconversion, therefore, involves only minor ligand motion and should take place, like that of the two 17-electron isomers examined above, with a minimal activation barrier. A second nonclassical singlet stereoisomer having the open site trans to the equatorial P atom is located 4.8 kcal/mol higher than the most stable classical structure. The two triplet geometries can be described as four-legged piano stools having cisoid (P trans to P, H trans to H_2) and transoid configurations, respectively. The transoid geometry is very similar to that of the nonclassical CpMoH(H2)(dpe)+ [compare Figure 10 and **Figure 11**(d)], the terminal Mo-H being shorter and all other distances longer in the more oxidized ion. The interconversion between these triplet isomers and the singlet may be more difficult than suggested by their mere energy difference, since a spin pairing process must take place. It is not clear-cut to establish which of these structures is the real ground state, because the energy changes caused by the computational level and the quality of the model are probably comparable or greater than the calculated energy differences.

Other intermediates and products of the proton transfer of pathway I

Complex $CpMoH_4(dpe)^+$, a model for the product of proton addition to $[Mo]H_3$, adopts a distorted pseudo-pentagonal bipyramidal geometry, as found in a parallel study for the same system[27] and also analogous to that previously calculated[9] for the related W system (see Figure 12(a)). This also corresponds to the experimentally determined structure of complex $[W]H_4^+$.[31] As discussed above, intermediate $[Mo]H_3^{2+}$ (or its nonclassical tautomer $[Mo]H(H_2)^{2+}$) of pathway I may either lose a proton or coordinate a MeCN molecule as the first step. The model system for the proton loss product, the 16-electron complex $CpMoH_2(dpe)^+$, adopts either a singlet or a triplet configuration like its protonated precursor examined above. In this case, the most stable structures are the triplets (Figure 12) whereas the singlet (not shown) is found 6.3 kcal mol^{-1} higher in energy. No nonclassical minima were located for this formulation.

The model for the MeCN addition product is most stable in the classical trihydride form, $CpMoH_3(dpe)(MeCN)^{2+}$. The MeCN ligand occupies an equatorial position in a distorted pseudo-pentagonal geometry, adjacent to one H ligand and the equatorial P donor [see Figure 13(a)]. This geometry can be seen as deriving from the straightforward addition of MeCN to the most stable geometry of $CpMoH_3(dpe)^{2+}$ (**Figure 11**). All Mo-ligand distances remain essentially unaltered upon MeCN addition. Three geometrically related nonclassical structures, however, are only slightly higher in energy. These are distorted pseudo-octahedral structures with the Cp center

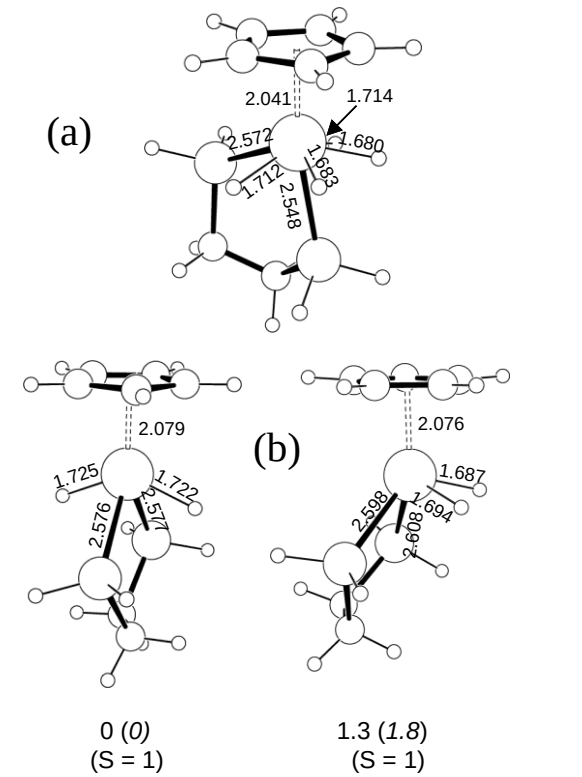

Figure 12 B3LYP/LANL2DZ-optimized geometries and gas phase (MeCN solution) relative energies in kcal mol^{-1} of complexes $[CpMoH_4(H_2PCH_2CH_2PH_2)]^+$ (a) and $[CpMoH_2(H_2PCH_2CH_2PH_2)]^+$ (b).

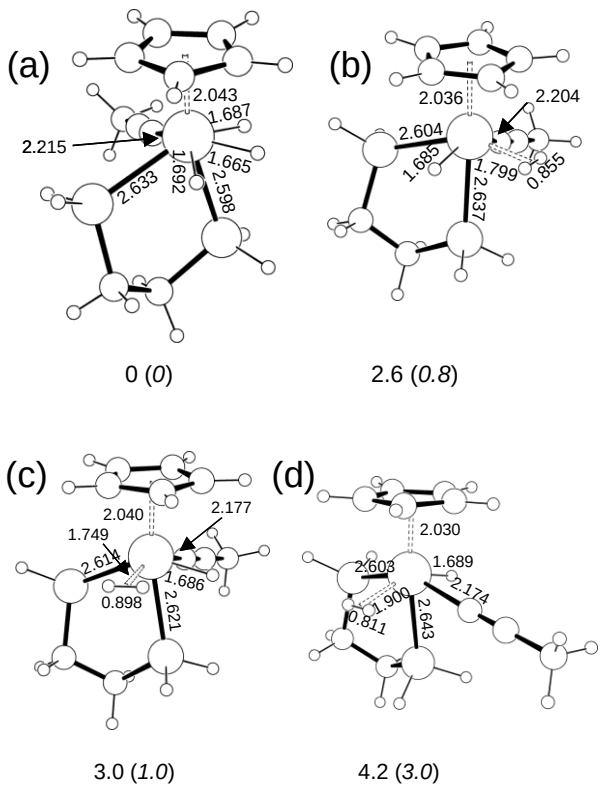

Figure 13 B3LYP/LANL2DZ-optimized geometries and relative gas phase (MeCN solution) energies in kcal mol^{-1} for $[CpMoH_3(H_2PCH_2CH_2PH_2)(MeCN)]^{2+}$.

and one P donor in the axial positions and may be distinguished by the ligand occupying the equatorial position trans to the second P donor: H_2 (*b*), +2.6 kcal/mol; H (*c*), +3.0 kcal/mol; and MeCN (*d*), +4.2 kcal/mol. These structures will be referred to below as isomer **a**, **b**, **c** and **d** according to the order they are presented in Figure 13. The nonclassical isomers **b** and **c** may be obtained from the most stable classical isomer **a** with minimal molecular rearrangements, leading to the hypothesis that they probably establish a rapid equilibrium. Isomer **d**, on the other hand, cannot be readily obtained by intramolecular motions from any of the other isomers. Given that the most stable 16-electron trihydride systems are the singlet classical and nonclassical ones in **Figure 11**(*a*) and (*b*), the straightforward MeCN addition to these species may be anticipated to lead preferentially to isomers **a** and **b** of the solvated product. Isomer **c** may be, as mentioned above, in rapid equilibrium with **a** and **b**, or could be directly obtained from the precursor in **Figure 11**(c) after spin pairing. Isomer **d**, on the other hand, may readily be obtained, after spin pairing, only from the precursor in **Figure 11**(*d*).

Finally, the $CpMoH_2(dpe)(MeCN)^+$ system adopts a distorted pseudo-octahedral geometry with the two hydrido ligands either *trans* or *cis* with respect to each other. The *cis* isomer is the most stable one by a fair amount (see Figure 14), probably a consequence of the electronic destabilization introduced by the two mutually *trans* hydrides. A comparison with the geometric parameters of the $CpMoH_3(dpe)(MeCN)^{2+}$ isomers (classical and nonclassical) in Figure 13 shows that the loss of a proton has the effect of shortening considerably the Mo-P, Mo-N and Mo-CNT bonds while the Mo-H bonds are lengthened.

Addition of MeCN to classical $CpMo(dpe)H_3^{+\bullet}$

As discussed above, one possibility envisaged for the electrochemical process B is oxidation of a 19-electron species, $[Mo]H_3(MeCN)^{+\bullet}$, deriving from the solvent addition to $[Mo]H_3^{+\bullet}$ (see Scheme 3, pathway *a*). Addition of MeCN to the classical structure leads to a stable minimum with a rather odd geometry, see Figure 15(a). This exhibits a very long Mo···N contact (4.158 Å), which is indicative of a charge-dipole interaction rather than a bonding interaction. The geometry of the metal fragment corresponds to the higher energy classical isomer of 17-electron $[CpMoH_3(dpe)]^{+\bullet}$ species (*C'* in Figure 10). In this structure, the Cp ring binds the metal in an essentially η^5 fashion (the individual Mo-C distances are in the 2.367-2.442 Å range). This minimum is located at 8.2 (gas phase) or 1.4 (MeCN solution) kcal/mol below the combination of the separate 17-electron trihydride and MeCN.

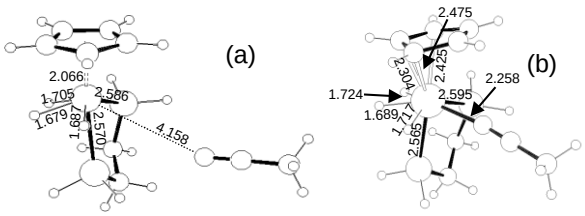

Figure 15 B3LYP/LANL2DZ-optimized geometries of complexes $[CpMH_3(MeCN)(H_2PCH_2CH_2PH_2)]^{+\bullet}$ (a: M = Mo; b: M = W).

The $[W]H_3$ complex also displays the same electrochemical process B, though at much reduced intensity (Figure 7). The 17-electron precursor had been calculated earlier at the same level of theory, the geometry being essentially identical to that of the classical Mo analogue.[9] The optimized geometry of the tungsten MeCN adduct differs substantially from that of the molybdenum counterpart, as shown in Figure 15(b). The acetonitrile ligand is now at a regular bonding distance from the metal center, while the Cp ring has slipped off to an essentially η^3 coordination mode, the two longer W-C distances not shown in the figure being 2.849 and 2.903 Å. The complex is essentially isoenergetic with the separate fragments (0.6 kcal/mole *less* stable). When the Mo system was optimized starting from the optimized geometry of the W system, the minimum of Figure 15(a) was again obtained.

This result disagrees with the hypothesis that this 19-electron complex is the source of peak B, because the experiment shows a *slow and quantitative* formation of the electroactive species for the Mo system, and a thermodynamically unfavorable one for the W system. The

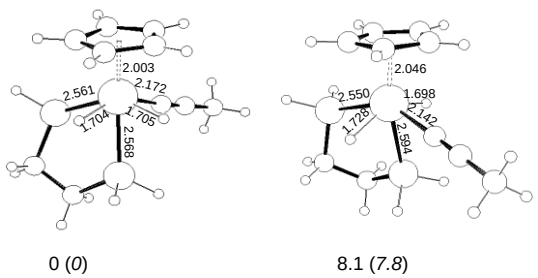

0 (*0*) 8.1 (*7.8*)

Figure 14 B3LYP/LANL2DZ-optimized geometries and relative gas phase (MeCN solution) energies in kcal mol^{-1} of complex $[CpMoH_2(H_2PCH_2CH_2PH_2)(MeCN)]^+$.

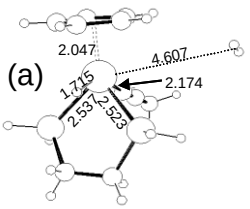

-11.4 (*-9.2*)

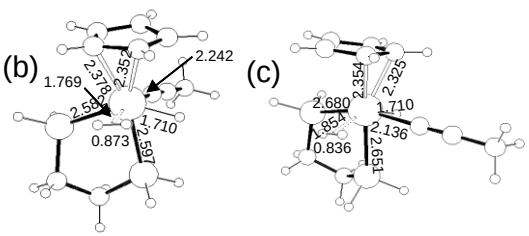

4.6 (*2.7*) 7.0 (*5.9*)

Figure 16 B3LYP/LANL2DZ-optimized geometries and gas phase (MeCN solution) energies in kcal mol^{-1}, relative to the classical isomer of Figure 15(a), of various $[CpMoH(H)_2(MeCN)(H_2PCH_2CH_2PH_2)]^{+\bullet}$ species.

minima of Figure 15 are not energetically very favorable and should be accessed quite rapidly from the individual components. It seems safe to conclude that this mechanistic hypothesis is wrong. As will be shown below, the alternative hypothesis (Scheme 3, pathway *b*) is in much greater harmony with the computational results.

Associative substitution of H_2 by MeCN in CpMo(dpe)H(H_2)$^{+\bullet}$

Three different minima were located for the nonclassical tautomer of the "19-electron" molybdenum complex, [Mo]H(H_2)(MeCN)$^{+\bullet}$, starting from each of the optimized nonclassical isomers of the 18-electron dication (isomers **b**, **c** and **d**) of Figure 13. Addition of one electron to isomer **b** (η^2-H_2 ligand trans to P) causes the spontaneous departure of the H_2 ligand and convergence to the structure illustrated in Figure 16(a), which corresponds to a van der Waals complex of CpMoH(dpe)(MeCN)$^{+\bullet}$ and H_2. Its energy is essentially the same as the sum of the energies of the separately optimized species. The CpMoH(dpe)(MeCN)$^{+\bullet}$ moiety adopts a *trans* four-legged piano stool geometry which is closely related, also in terms of bond distances, to that of the isoelectronic CpMoH(H_2)(dpe)$^{+\bullet}$ shown in Figure 10. The Cp ligand is again essentially symmetrically bonded to the metal atom (2.361-2.417 Å). On the other hand, adding an electron to isomers **c** and **d** (η^2-H_2 trans to MeCN and H, respectively) yields geometries where the H_2 ligand remains bonded to the metal atom while the Cp ring becomes asymmetrically bonded. The geometry of the MoH(H_2)(dpe)(MeCN) moiety remains essentially unchanged from that shown in the corresponding dication, except for minor variation in the bond distances [*cf.* Figure 13(c) with Figure 16(b) and Figure 13(d) with Figure 16(c)]. The Mo-C distances, on the other hand, span a large range in each case, the longer distances not shown in the figure being 2.557, 2.817 and 2.634 Å for the isomer in Figure 16(b) and 2.566, 2.859 and 2.679 Å for the isomer in Figure 16(c). These local minima are at higher energy relative to the classical isomer, but still lower than the sum of free CpMoH(H_2)(dpe)$^{+\bullet}$ and MeCN. The geometry of the reaction product of the ligand substitution, namely the 17-electron [Mo]H(MeCN)$^{+\bullet}$, is identical to that obtained by the spontaneous expulsion of H_2 starting from 19-electron [Mo]H(H_2)(MeCN)$^{+\bullet}$ (Figure 16(a)). Thus, it is possible to predict that the associative exchange of H_2 with MeCN (pathay *b* of Scheme 3) will occur readily. The energy profile of this exchange is shown in Figure 17.

The 15-electron CpMo(dpe)H$^+$ system

The alternative proposition for the exchange of H_2 with acetonitrile from [Mo]H(H_2)$^{+\bullet}$ involves a dissociative mechanism via the 15-electron [Mo]H$^+$ intermediate. The latter could in principle adopt either a doublet or a quartet state,[32, 33] since the orbital left vacant by the H_2 dissociation could serve to host an electron following the unpairing of a metal lone pair. The calculations show that this highly unsaturated intermediate is more stable as a spin quartet, and that the energy required for the H_2 dissociation from the [Mo]H(H_2) $^{+\bullet}$ precursor is only 11.4 (gas phase or 11.7 (MeCN solution) kcal mol^{-1}, see Figure 17. Thus, this substitution pathway is predicted by the calculation to be relative facile. However, this mechanism remains less favorable than the associative mechanism examined above, at least in the absence of significant steric bulk. The geometries of the two 15-electron intermediates are quite close to each other. Both the Mo-CNT and Mo-P distances are slightly longer in the higher-spin system as expected, whereas the Mo-H distance is exactly the same for both systems.

Further mechanistic considerations

Both possible pathways for the transformation of Scheme 2 (proton transfer followed by MeCN coordination, or viceversa) are examined again in Scheme 5 in terms of the calculated total energies. The direct and irreversible proton transfer from [Mo]H_3^{2+} to [Mo]H_3 (first step for pathways *a* and *c* of Scheme 2) is calculated as the more exoergic

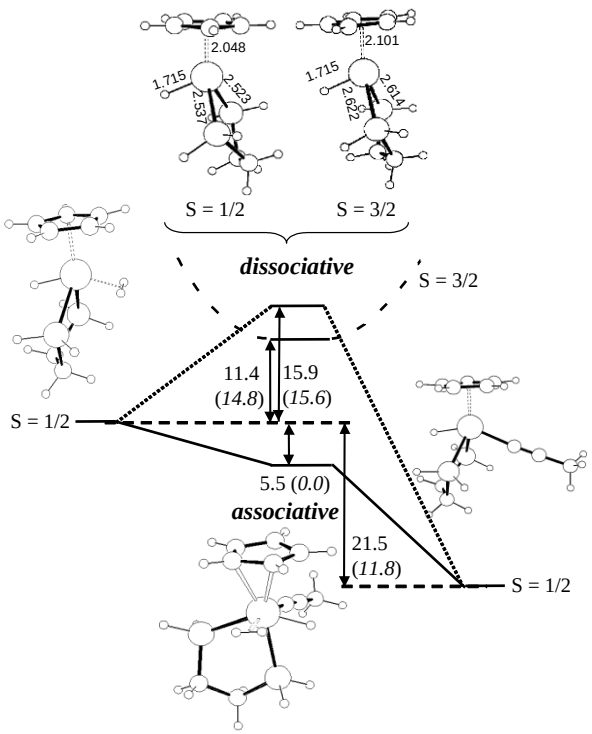

Figure 17 B3LYP/LANL2DZ-optimized geometries and relative gas phase (MeCN solution) energies in kcal mol^{-1} for the transformation of [CpMoH(H_2)(H_2PCH_2CH_2PH_2)]$^{+\bullet}$ and MeCN to [CpMoH(MeCN)(H_2PCH_2CH_2PH_2)]$^{+\bullet}$ and H_2.

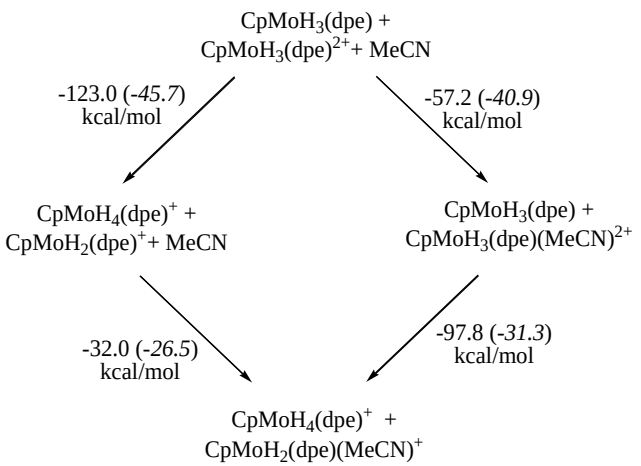

Scheme 5

possibility for the model system, being downhill by 45.7 kcal/mol in MeCN solution (123.0 kcal/mol in the gas phase). Note that the PCM has a very large effect on this energy, since the process transforms a neutral and a doubly charged species into two singly charged species. A doubly charged species is expected to be far most stabilized by solvation than the sum of two singly charged species. Only the MeCN solution values will be further discussed. The subsequent MeCN coordination to the $CpMoH_2(dpe)^+$ intermediate takes the system further down in energy by 26.5 kcal/mol, for a total energy difference of 72.2 kcal/mol. The alternative pathway (*b* of Scheme 2) involves acetonitrile coordination to the $[Mo]H_3^{2+}$ complex for a gain of 40.9 kcal/mol, followed by the proton transfer process which is exoergic by 31.3 kcal/mol. The calculations suggest that the most probable first step of the process is proton transfer from $[Mo]H_3^{2+}$ to $[Mo]H_3$. Since the kinetic data exclude that this is the rate determining step (*vide supra*), the remaining possibility is that illustrated in pathway *c*, *i.e.* a fast proton transfer followed by a rate determining MeCN coordination. In other words, after the second oxidation step, the hydride compound becomes so acidic that the deprotonation process becomes a very favorable process. Therefore, it is likely to be quantitative rather than an equilibrium process. It is in fact quite possible that the proton is transferred in a first rapid process from $[Mo]H_3^{2+}$ to the surrounding MeCN solvent and subsequently delivered from $MeCNH^+$ to the $[Mo]H_3$ base.

On the basis of the theoretical calculations shown above, it is possible to speculate further. The rearrangement of $[Mo]H_3^{2+}$ to its nonclassical isomer $[Mo]H(H_2)^{2+}$ [Figure 13(*b*)] is likely to be very fast and both isomers are calculated as essentially isoenergetic. Furthermore, although the pK_a values of tautomeric classical and nonclassical polyhydrides are usually rather similar,[34] nonclassical hydride complexes are often kinetically more acidic than their classical counterparts.[17, 34, 35] Therefore, it seems quite likely that the proton transfer occurs via the $[Mo]H(H_2)^{2+}$ complex and the involvement of this rapid interconversion is included in path I of Scheme 4. Furthermore, the electrochemical mechanistic study excludes that either $[Mo]H_3^{2+}$ or $[Mo]H(H_2)^{2+}$ coordinate MeCN in a rate determining step before being deprotonated. According to the calculations, these processes would lead straightforwardly to isomers **a** and **b**, respectively, of system $[Mo]H_3(MeCN)^{2+}$ (Figure 13) with consequent H_2 elimination and generation of species $[Mo]H(MeCN)_2^{2+}$, which is responsible for process F. The lack of such competitive solvent addition processes rationalizes why, upon fast scan rate voltammetry beyond the second oxidation process D (*i.e.* when no sufficient time is allowed for pathways II and III to occur), peak F is not observed in the voltammogram.

The striking acidity difference between $[Mo]H(H_2)^{2+}$ (pathway I, only deprotonation leading to process C) and $[Mo]H(H_2)S^{2+}$ (pathway III, only H_2 elimination leading to process F) must be related to the buffering effect of the acetonitrile coordination on the H_2 ligand acidity. Conversely, the more saturated configuration of the acetonitrile adduct certainly favors the H_2 elimination. A rough estimate of the acidity decrease is possible on the basis of the computational results. The proton transfer process from $[Mo]H(H)_2^{2+}$ to $[Mo]H_2S^+$ yielding $[Mo]H_2^+$ and $[Mo]H(H)_2S^{2+}$ is exoergic by 12.0 kcal/mol in MeCN solution. Equating this value to the standard free energy, with all related approximations as discussed above, yields an acid dissociation constant for $[Mo]H_3S^{2+}$ which is ca. 9 orders of magnitude smaller than that of $[Mo]H_3^{2+}$.

The computational results presented here also allow us to further comment the previously discussed pathways.[9] The primary product of pathway II in Scheme 4, *i.e.* the deprotonation product of $[M]H(H_2)^{+\bullet}$, is the neutral 17-electron species $[M]H_2^{\bullet}$. Previous studies for monohydride complexes MH[8, 11, 22, 36] have shown that the 17-electron product of formal H atom abstraction, $M^{\bullet}$, is much easier to oxidize than its 18-electron MH precursor (by about –1.3 V). This oxidation is probably preceded by solvent coordination. Although we have no direct experimental evidence, the same evolution can be postulated for the trihydride compound, *i.e.* complex $[M]H_2^{\bullet}$ is immediately oxidized under the condition in which it forms. This leads to the formation of complex $[M]H_2S^+$ which is responsible for wave C. The deprotonation pathway is very slow in MeCN (it was only detected by a thin-layer CV study at scan rates < ca. 10 mV s^{-1}).[9] This is the reason why the presence of wave C during the first scan is only observed at very slow scan rates.

A comparison of the oxidation potentials of the different 18-electron complexes $[Mo]H_3$, $[Mo]H_2S^+$ and $[Mo]HS_2^{2+}$ (peaks A, C and F, respectively) shows that the nature of the ligands strongly affects the ability of the complexes to be oxidized: The oxidation potential increases in the order $E°([M]H_3) < E°([M]H_2S^+) < E°([M]HS_2^{2+})$. This trend reflects the greater donating power of a H^- ligand relative to MeCN. The potential for the oxidation of $[Mo]H_2^{\bullet}$ (< E_A) and $[Mo]HS^{+\bullet}$ (E_B) follow the same trend. A change of metal from Mo to W does not greatly alter the oxidation potential of waves A, B, C and D (wave F was never observed for the W system). Since the disproportionation pathway occurs only upon rearrangement to the nonclassical structure, the oxidation of the non-classical solvent adduct $[MoH(H_2)S]^{+\bullet}$ must lie at a less positive potential than process A. This potential (which cannot be measured directly) can be calculated from Equation 8, since the disproportionation equilibrium constant (K_{Disp}= > 10^{10}) is estimated from our previous study.[9] The resulting value is more negative than

$$E^{o}_{[MH(H_2)S]^{+\cdot}/[MH(H_2)S]^{2+}} = E^{o}_{MH_3/[MH_3]^{+\cdot}} - \frac{2.3RT}{F}\log K_{Disp} \quad (8)$$

wave A (by > 600 mV), as expected.

Conclusions

Our work constitutes a complete study of the decomposition mechanism of the 17-electron trihydride complexes $[Cp^*MH_3(dppe)]^{+\bullet}$ (M = Mo, W) in the presence of acetonitrile. Even though quite complex, the complete picture in Scheme 4 satisfactorily rationalizes all the observed chemical and electrochemical behavior while being compatible with the results of the theoretical calculations.

The present study has highlighted the following new aspects of paramagnetic hydride chemistry.

The double oxidation of the title trihydride complex induces an immediate proton transfer to the starting complex, followed by rate determining solvent coordination.

The oxidatively induced H_2 reductive elimination from a polyhydride complex has been quantitatively assessed in MeCN. This process competes with solvent coordination followed by disproportionation and slow proton transfer. From the computational point of view, it seems possible that this process occurs via a dissociative 15-electron species, which would adopt a spin quartet ground state.

The addition of an acetonitrile molecule is shown to dramatically reduce the acidity of the oxidized hydride complex.

Continuing work in this area must address the effect of the metal oxidation on the fundamental properties (polarity, polarizability, homolytic bond strength) of the M-H bond(s), an area where there is still precious little information,[8] in order to develop new molecules for catalytic and electrocatalytic applications by rational design.

Experimental

General. Compounds $Cp^*M(dppe)H_3$ (M = Mo, W), $[Cp^*Mo(dppe)H_2(MeCN)]^+$ and $[Cp^*Mo(dppe)H(MeCN)_2]^{2+}$ have been prepared as previously described.[31] All manipulations were carried out under an inert atmosphere of dinitrogen or argon by the use of Schlenk line or glove box techniques. THF was distilled under dinitrogen prior to use. MeCN (HPLC grade) was carefully dried by percolation on neutral alumina that had been activated for 8 h under vacuum at 220°C.

Electrochemistry. Cyclic voltammograms were carried out in a three-electrode cell with an EG&G 283 potentiostat connected to a PC. The working electrode was a 1.5 mm diameter platinum disk, the counter electrode a platinum wire and the reference a BAS Ag / AgCl electrode (- 35 mV / SCE) separated from the solution by a glass chamber with a porous vycor tip filled up with a saturated solution of Bu_4NPF_6 in MeCN. Bu_4NPF_6 was used as supporting electrolyte at a concentration of 0.2 M. The experiments were carried out at 20°C. All electrochemical potentials are given relative to Ag/AgCl (3 M). The $E_{1/2}$ found for ferrocene under the present condition is +0.51 V.

Computational details. Most calculations were carried out on model compounds were the Cp* ligand was replaced by Cp and the dppe ligand was replaced by $PH_2CH_2CH_2PH_2$. The calculations were performed using the Gaussian03 program package[37] under the DFT approach by using the B3LYP functional[38] and the LANL2DZ basis set.[39-42] Larger systems containing the real dppe ligand (but with the Cp still being modeled by the simpler Cp ligand) were also optimized for the $[Mo]H_3^{+\bullet}$ and $[Mo]H(H_2)^{+\bullet}$ structures and for the transition state interconverting them. These calculations were carried out at the full QM level, but the C and H atoms of the four phenyl rings were described by the simpler STO-3G basis functions, whereas all other atoms were treated by the LANL2DZ basis set as for the simpler model. The calculations in the MeCN medium (ε = 36.64) were carried out on the gas-phase optimized structures with the polarizable continuum model (PCM),[28] using standard options of PCM and cavity keywords.[37] All geometries were fully optimized without symmetry restrictions and were characterized as local minima or transition states of the potential energy surface (PES) by inspection of the sign of the second derivatives. The mean value of the S^2 operator was always very close to the theoretical value of 0.75 for spin doublets, 2 for spin triplets, and 3.75 for spin quartets indicating minor amounts of spin contamination. In all cases, energies are given in kcal mol^{-1}. The reported energy values do not include a correction for the zero-point vibrational energy (ZPVE), whereas the reported free energy values include ZPVE, PV and TS contributions at 298 K.

Acknowledgement

We are grateful to the European Commission for sponsoring this research through the HYDROCHEM Research Training Network (Contract n° HPRN-CT-2002-00176) and CINES for granting us free computer time. MB thanks the Spanish Ministerio de Educación y Ciencia for a post-doctoral fellowship.

Notes and references

1. A. Maeland, in *Recent Advances in Hydride Chemistry*, eds. R. Poli and M. Peruzzini, Elsevier Science, Amsterdam, Editon edn., 2001.
2. G. W. Parshall, *Homogeneous Catalysis: The Applications and Chemistry of Catalysis by Soluble Transition Metal Complexes*, John Wiley and Sons, New York, 1980.
3. G. J. Kubas, R. R. Ryan, B. I. Swanson, P. J. Vergamini and H. J. Wassermann, *J. Am. Chem. Soc.*, 1984, **106**, 451-452.
4. G. J. Kubas, *Acc. Chem. Res.*, 1988, **21**, 120-128.
5. R. H. Crabtree, *Acc. Chem. Res.*, 1990, **23**, 95-101.
6. P. G. Jessop and R. H. Morris, *Coord. Chem. Rev.*, 1992, **121**, 155-284.
7. D. M. Heinekey and W. J. Oldham, *Chem. Rev.*, 1993, **93**, 913-944.
8. R. Poli, in *Recent Advances in Hydride Chemistry*, eds. R. Poli and M. Peruzzini, Elsevier Science, Amsterdam, Editon edn., 2001, pp. 139-188.
9. B. Pleune, D. Morales, R. Meunier-Prest, P. Richard, E. Collange, J. C. Fettinger and R. Poli, *J. Am. Chem. Soc.*, 1999, **121**, 2209-2225.
10. C. Bianchini, F. Laschi, M. Peruzzini, F. Ottaviani, A. Vacca and P. Zanello, *Inorg. Chem.*, 1990, **29**, 3394-3402.
11. O. B. Ryan, M. Tilset and V. D. Parker, *J. Am. Chem. Soc.*, 1990, **112**, 2618-2626.
12. D. H. Vaughan, in *Comprehensive Coordination Chemistry. The Synthesis, Reactions, Properties and Applications of coordnation Compounds*, ed. S. G. Wilkinson, Pergamon Press, Oxford, Editon edn., 1987, vol. 1, p. 503.
13. C. K. Mann, in *Electroanalytical Chemistry. A Series of Advances.*, ed. A. J. Bard, Marcel Dekker, New york, Editon edn., 1969, vol. 3, pp. 57-134.

14. P. Delahay, *New Instrumental Methods in Electrochemistry. Theory, Instrumentation and Applications to analytical and Physical Chemistry*, R. E. Krieger, New York, 1980.
15. C. P. Andrieux and J. M. Savéant, in *Investigation of Rates and Mechanisms of Reactions, Part II*, ed. C. Bernasconi, John Wiley & Sons, New York, Editon edn., 1986, vol. VI, pp. 305-390.
16. M. S. Chinn and D. M. Heinekey, *J. Am. Chem. Soc.*, 1990, **112**, 5166-5175.
17. G. Jia, A. J. Lough and R. H. Morris, *Organometallics*, 1992, **11**, 161-171.
18. E. T. Papish, F. C. Rix, N. Spetseris, J. R. Norton and R. D. Williams, *J. Am. Chem. Soc.*, 2000, **122**, 12235-12242.
19. A. E. Stiegman and D. R. Tyler, *Comments Inorg. Chem.*, 1986, **5**, 215-245.
20. C. E. Philbin, C. A. Granatir and D. R. Tyler, *Inorg. Chem.*, 1986, **25**, 4806-4807.
21. M. J. Therien and W. C. Trogler, *J. Am. Chem. Soc.*, 1987, **109**, 5127-5133.
22. D. R. Tyler, *Acc. Chem. Res.*, 1991, **24**, 325-331.
23. Y. Zhang, D. K. Gosser, P. H. Rieger and D. A. Sweigart, *J. Am. Chem. Soc.*, 1991, **113**, 4062-4068.
24. R. S. Nicholson and J. Shain, *Anal. Chem.*, 1964, **36**, 706-723.
25. K. M. Smith, R. Poli and J. N. Harvey, *Chem. Eur. J.*, 2001, **7**, 1679-1690.
26. O. Salomon, M. Reiher and B. A. Hess, *J. Chem. Phys.*, 2002, **117**, 4729-4737.
27. N. V. Belkova, P. O. Revin, M. Besora, M. Baya, L. M. Epstein, A. Lledós, R. Poli, E. S. Shubina and E. V. Vorontsov, *Eur. J. Inorg. Chem.*, in press.
28. J. Tomasi and M. Persico, *Chem. Rev.*, 1994, **94**, 2027-2094.
29. Z. Y. Lin and M. B. Hall, *Coord. Chem. Rev.*, 1994, **135**, 845-879.
30. F. Maseras, A. Lledós, E. Clot and O. Eisenstein, *Chem. Rev.*, 2000, **100**, 601-636.
31. B. Pleune, R. Poli and J. C. Fettinger, *Organometallics*, 1997, **16**, 1581-1594.
32. R. Poli, *Chem. Rev.*, 1996, **96**, 2135-2204.
33. R. Poli, *J. Organomet. Chem*, 2004, **689**, 4291–4304.
34. K. Abdur-Rashid, T. P. Fong, B. Greaves, D. G. Gusev, J. G. Hinman, S. E. Landau, A. J. Lough and R. H. Morris, *J. Am. Chem. Soc.*, 2000, **122**, 9155-9171.
35. G. Jia and R. H. Morris, *Inorg. Chem.*, 1990, **29**, 581-582.
36. F. Marken, A. M. Bond and R. Colton, *Inorg. Chem.*, 1995, **34**, 1705-1710.
37. M. J. Frisch, G. W. Trucks, H. B. Schlegel, G. E. Scuseria, M. A. Robb, J. R. Cheeseman, J. Montgomery, J. A., T. Vreven, K. N. Kudin, J. C. Burant, J. M. Millam, S. S. Iyengar, J. Tomasi, V. Barone, B. Mennucci, M. Cossi, G. Scalmani, N. Rega, G. A. Petersson, H. Nakatsuji, M. Hada, M. Ehara, K. Toyota, R. Fukuda, J. Hasegawa, M. Ishida, T. Nakajima, Y. Honda, O. Kitao, H. Nakai, M. Klene, X. Li, J. E. Knox, H. P. Hratchian, J. B. Cross, C. Adamo, J. Jaramillo, R. Gomperts, R. E. Stratmann, O. Yazyev, A. J. Austin, R. Cammi, C. Pomelli, J. W. Ochterski, P. Y. Ayala, K. Morokuma, G. A. Voth, P. Salvador, J. J. Dannenberg, V. G. Zakrzewski, S. Dapprich, A. D. Daniels, M. C. Strain, O. Farkas, D. K. Malick, A. D. Rabuck, K. Raghavachari, J. B. Foresman, J. V. Ortiz, Q. Cui, A. G. Baboul, S. Clifford, J. Cioslowski, B. B. Stefanov, G. Liu, A. Liashenko, P. Piskorz, I. Komaromi, R. L. Martin, D. J. Fox, T. Keith, M. A. Al-Laham, C. Y. Peng, A. Nanayakkara, M. Challacombe, P. M. W. Gill, B. Johnson, W. Chen, M. W. Wong, C. Gonzalez and J. A. Pople, *Gaussian 03, Revision B.04*, Gaussian, Inc., Pittsburgh PA, 2003.
38. A. D. Becke, *J. Chem. Phys.*, 1993, **98**, 5648-5652.
39. T. H. Dunning, Jr. and P. J. Hay, in *Modern Theoretical Chemistry*, ed. H. F. Schaefer, III, Plenum Press, New York, Editon edn., 1976, pp. 1-28.
40. P. J. Hay and W. R. Wadt, *J. Chem. Phys.*, 1985, **82**, 270-283.
41. P. J. Hay and W. R. Wadt, *J. Chem. Phys.*, 1985, **82**, 299-310.
42. W. R. Wadt and P. J. Hay, *J. Chem. Phys.*, 1985, **82**, 284-298.